Computational Screening for Selective Catalysts: Cleaving the C–C Bond During Ethanol Electro-Oxidation Reaction

*Evans A. Monyoncho [1], Stephan N. Steinmann [2], Philippe Sautet, [3,4] Elena A. Baranova, [1, *]*

*Carine Michel [2, *]*

1. Department of Chemical and Biological Engineering, Centre for Catalysis Research and Innovation (CCRI), University of Ottawa, Ottawa, Ontario K1N 6N5, Canada

2. Univ Lyon, ENS de Lyon, CNRS UMR 5182, Université Claude Bernard Lyon 1, Laboratoire de Chimie, F69342, Lyon, France

3. Department of Chemistry and Biochemistry, University of California, Los Angeles (UCLA), Los Angeles, California, 90095, United States

4. Department of Chemical and Biomolecular Engineering, University of California, Los Angeles (UCLA), Los Angeles, California, 90095, United States

* Elena.Baranova@uottawa.ca

* carine.michel@ens-lyon.fr

Abstract

The efficiency of direct ethanol fuel cells suffers from the partial oxidation of ethanol into acetic acid as opposed to the complete oxidation of this fuel to CO_2. Herein, we support the quest for a selective catalyst for ethanol electro-oxidation to CO_2, building on our previous mechanistic hypothesis based on experimental insight and DFT computations. We derive a simple descriptor of the expected selectivity towards full oxidation, Ω, as a function of the adsorption energy of atomic C and O. Three different families of catalyst surfaces are screened using this descriptor: monometallics, bimetallics and conducting metal oxides, totaling to 600 surfaces. In agreement with available experimental data, no single metal surface is more selective for total oxidation than platinum and palladium. While the selected conducting oxides were not predicted to be selective towards splitting the C–C bond, structurally-controlled monometallics (such as Pd(100)) or some bimetallics (Pd_3Ag) are found to be competitive with the most stable facet, (111), of Pd and Pt. Despite this very extensive screening, no very promising catalyst has been identified. This highlights the need to identify catalysts for acetate oxidation or to exploit support effects and electrolyte engineering to profit from the full power of direct ethanol fuel cells.

2

Introduction

Direct ethanol fuel cells are promising for a number of reasons: i) ethanol is a non-toxic liquid, which lowers the investment of handling facilities because the current infrastructure for gasoline can be largely used, ii) ethanol can be conveniently produced from biomass, hence is carbon neutral which mitigates the increasing atmospheric CO_2, iii) ethanol is the smallest alcohol with the C–C bond, hence can serve as a model for the electro-oxidation of bigger compounds containing the C–C bonds, iv) ethanol has a higher energy density than methanol if completely oxidized to CO_2 since it can deliver 12 electrons per molecule.[1–3] However, the C–C bond resists scission and the oxidation of ethanol usually stops at the production of acetic acid, limiting the energy efficiency of this non-toxic alcohol for fuel cell applications.

An overview of the advances in the study of ethanol electrooxidation mechanism and the electrocatalytic materials with a focus on Pt- and Pd-based catalysts is provided Wang *et al*.[4] They reported that consensuses from the mechanistic studies are that sufficient active surface sites to facilitate the cleavage of the C–C bond and the adsorption of water or water residue were critical for obtaining higher activity. They showed how this understanding had been applied to achieve improved performance on various Pt- and Pd-based catalysts by the optimization of electronic and bifunctional effects, as well as by tuning the surface composition and structure of the catalysts. Akhairi and Kamarudin published an overview of the acidic and alkaline DEFCs which focused on the work done on Pt and Pd and highlighted the outstanding problems such as the incomplete oxidation of ethanol to carbon dioxide and the need to control the selectivity of the reaction among others.[1]

For example, Lai *et al.* investigated EOR on Pt in electrolytes of varying pH and composition using electrochemical and surface-enhanced Raman spectroscopy (SERS) techniques.[5] According to their report, the reaction selectivity depends strongly on the nature of the electrolyte but to a smaller extent on the electrolyte pH.[5] Further investigations, revealed that the cleavage of the C–C bond was only observed on Pt in the absence of strongly adsorbed anions, which was attributed to the competition for the active sites. Cremers *et al.* have pointed out that the challenge in implementing DEFCs in acidic conditions was to oxidize acetaldehyde further, a step that was particularly difficult as it must not proceed via acetic acid which cannot be oxidized further to CO_2.[6] But in alkaline media, they found EOR to proceed rather faster and lead to a complete oxidation to CO_2, a promising approach for DEFCs.[7] Fang *et al.* studied EOR on a Pd electrode mechanism in alkaline solution.[8] They reported acetate was the main product for concentrations higher than 0.5 M NaOH and the C–C bond cleavage to form CO_2, occurred at pH ≤ 13 which was in agreement with online mass-spectrometry the results from Cantane and Lima evidencing CO_2 production over Pt and Pd in 0.01 M NaOH where acetic acid formation was almost absent.[9] Christensen *et al.* have shown that the interfacial pH drops at higher potentials due to the high consumption of OH^- which is not completely counterbalanced by the OH^- diffusion from the bulk-phase.[10–12] This phenomenon leads to a transition from alkaline to acidic conditions at the interphase. The transition potential varies with the diffusion rate of OH^- which is dependent on the temperature and mass flow-rate.

To support the quest for efficient selective catalysts, we recently focused on the ethanol oxidation at a Pd-based anode, combining periodic Density Functional Theory (DFT) and the Computational Hydrogen Electrode (CHE) model[13] with advanced interfacial infrared spectroscopy (PM-IRRAS).[14] In line with other experimental studies,[15–17,10,11,7,18,19] we found that a

4

potential improvement in the selectivity lies in the competition between two routes represented schematically in Figure 1.
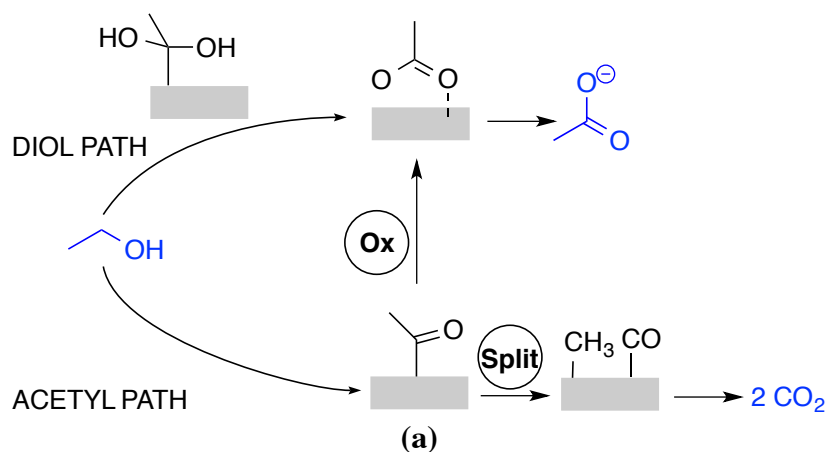

(a)

Figure 1: Simplified scheme of the most important intermediates and reaction paths for ethanol electro-oxidation mechanism. The blue species are the reactants and products, while the black species are the key intermediates as demonstrated in ref[14]. The selectivity towards the full oxidation results from the competition between acetyl oxidation into acetate (**Ox**) and its fragmentation into CH_3 and CO (**Split**)

In the diol pathway, acetate is readily formed from the diol intermediate ($CH_3C(OH)_2$) and then desorbs into the electrolyte. Currently, we are not aware of any efficient electrocatalyst for further oxidation of acetic acid oxidation or C–C scission in the diol pathway. In the acetyl pathway, the acetyl intermediate (CH_3CO) is pivotal in the control of the selectivity. On Pd, it is more stable than the diol but more difficult to reach.[14] Once produced, acetyl intermediate can either be further oxidized to acetate by C–OH coupling, or broken into CH_3 and CO fragments, opening the door to a complete oxidation of ethanol to CO_2. The oxidation by C–OH coupling is an electrochemical step that is facilitated by overpotential and by the presence of surface hydroxyls. On monometallic surfaces, the C–C splitting is greatly facilitated by the production of CO and cannot occur earlier in the reaction pathway.[20,21] In other words, the acetyl intermediate is the bottleneck to a selective process towards a full oxidation of ethanol as a fuel. Although the acetyl pathway opens the door to the C–C splitting, it is difficult to reach, and it is easily

oxidized to acetate, which is a dead end. On Pd, only less than 1% of ethanol is fully oxidized to CO_2 and H_2O in alkaline media according to our experimental results.[14]

In this article, we aim at supporting the quest for catalysts which are selective for splitting the C–C bond using *in-silico* screening using ethanol as the model molecule. The study endeavors to establish the rationale behind experimental reports that supported Pt and Pd nanoparticles are currently the most efficient EOR electrocatalysts [4] and the potential to reach better selectivity. To complement the several strategies proposed in the literature such as the inclusion of promoters (Sn, Ru or Rh etc.) and the use of alternative catalyst supports (CeO_2, TiO_2, SnO_2, etc.)[22,23] that show metal-support interaction (MSI) effects,[24,25] we have screened for bimetallics and metal oxides from a database of more than 600 entries.

Methodology

Density functional theory calculations were performed with the Vienna *Ab-initio* Simulation Package (VASP version 5.3.3).[26] The generalized gradient approximation of Pardew, Burke, and Erzenhorf (PBE)[27] was used to compute the exchange-correlation energy. The projector augmented wave (PAW) method [28] was employed to describe the core-electron interaction. A plane-wave basis set with an energy cut-off set to 400 eV was used. The metallic surfaces were modeled by a periodic slab with a p(3x3) unit cell containing five layers and separated from periodic images by a vacuum region of 10 Å. A 7 x 7 x 1 Monkhorst-Pack *k*-points mesh was employed for the Brillouin zone integration together with the second order Methfessel-Paxton smearing method[29] with a sigma of 0.2 eV. All optimizations were carried out to forces below 0.02 eV/Å, while the bottom three layers were kept fixed. Transition states were obtained by the combination of Nudge Elastic Band and Dimer algorithms and confirmed by the presence of a

unique imaginary frequency. The electrochemical potential effect was included using the computational hydrogen electrode.[13] For example, the reaction energy of the chemical reaction:

$$CH_3CH_2OH + H_2O + M \rightarrow CH_3COO@M + 5\ H^+ + 5e^-$$

is computed as

$$\Delta E = E_{(CH3COO)} + 2.5\ E_{(H2)} - (E_{(CH3CH2OH)} + E_M + E_{H2O}) - 5\ qU$$

Where q is the elemental charge and we have assumed U to be with respect to the pH insensitive RHE.

The adsorption of atomic C and O is done on a p(2x2) slab of 5 layers, keeping a 7 x 7 x 1 Monkhorst-Pack k-points mesh. The alloys considered are of the A_3B type, derived from the monometallic fcc metal. The (111) slab is cut from the optimized bulk position and exposes an external surface with 3 A atoms and 1 B atom in a primitive cell that is derived from the p(2x2) of the monometallic, following the approach of F. Studt et al.[30] A typical cell is shown in Figure 2 for Pd_3Ag. The bare (110) oxide surfaces were modeled by a symmetric periodic slab with a p(1x1) unit cell of three layers (around 10 Å) separated by 15 Å of vacuum as cleaved from the optimized bulk (error less than 1% compared to experiment for the norm of the cell vectors). A typical cell is shown in Figure 2 for RuO_2. A 3 x 3 x 1 Monkhorst-Pack k-points mesh was employed for the Brillouin zone integration together with a Gaussian smearing with a width of 0.05 eV, except for the SnO_2(110) surface where a denser grid of 5 x 5 x 1 was found to be necessary.

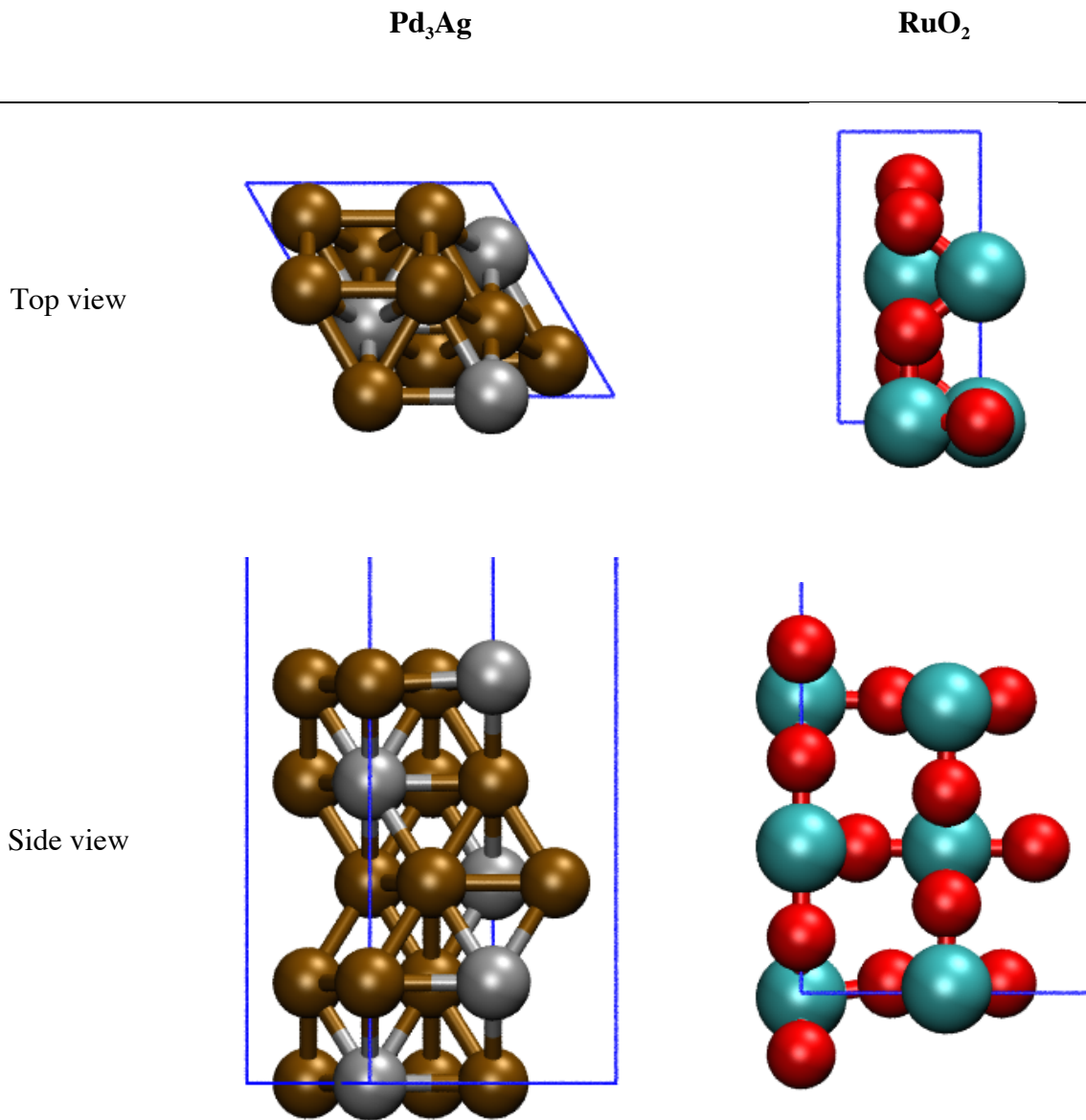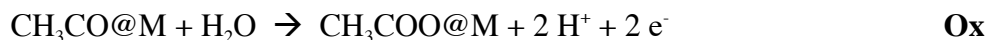|	**Pd₃Ag**	**RuO₂**

Pd₃Ag RuO₂

Top view

Side view

Figure 2: Top view and side view of typical simulation cells for metals (p(2x2) cell of Pd₃Ag(111)) and oxides (p(1x1) cell of RuO₂(110) surface) ; Pd is shown in ochre, Ag in gray, O in red, Ru in cyan, the cell boundaries in blue, the vacuum part is not fully represented.

Results and discussion

To improve the selectivity of a catalyst towards breaking the C–C bond during the ethanol electrooxidation, it is necessary to favor the formation of adsorbed acetyl and its fragmentation into CH_3 and CO (see Figure 1). Using DFT simulations, we focus here on the two main competing reactions, which consume acetyl species during ethanol electro-oxidation, i.e., the acetate formation (**Ox**), and the C–C bond cleavage (**Split**) reactions:

$$CH_3CO@M + H_2O \rightarrow CH_3COO@M + 2\ H^+ + 2\ e^- \qquad \textbf{Ox}$$

$$CH_3CO@M \rightarrow CH_3@M + CO@M \qquad \textbf{Split}$$

First, we explore the binding mode for acetate and acetyl on a broad range of transition metal surfaces (Re, Ru Os, Co, Rh, Ir, Ni, Pd, Pt, Cu, Ag, Au; see Table S1). Acetyl binds via C on top site on the 12 metal surfaces under consideration; hence a linear correlation is observed for acetyl vs C binding energy E_c with a mean average error of 0.10 eV (see Figure 3, top panel). Acetate adsorbs in a bi-dentate mode via the O atoms and its binding energy scales with the one of atomic oxygen E_o with a mean average error of 0.12 eV (see Figure 3, bottom panel).
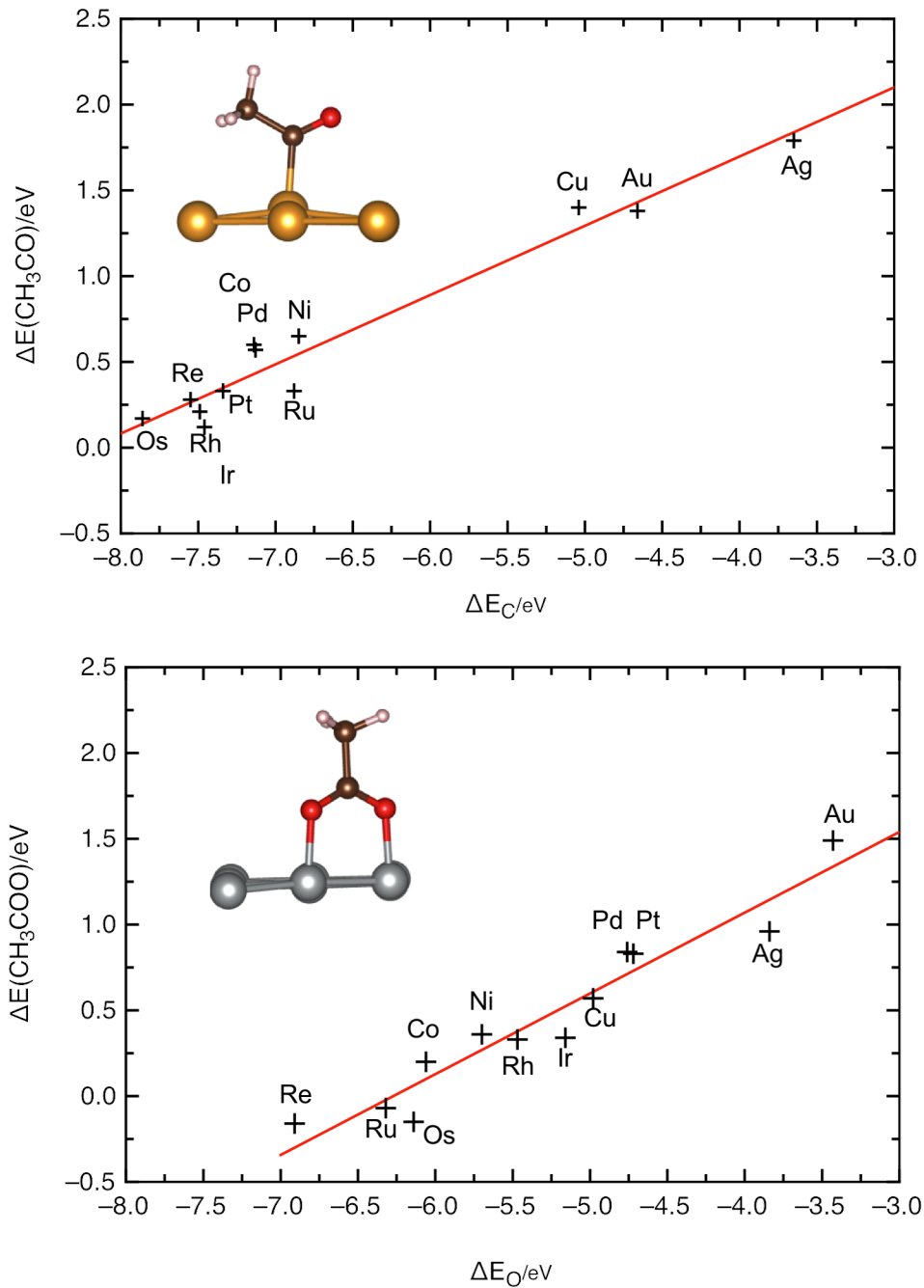
Figure 3. The energy of the acetyl CH_3CO and the acetate CH_3COO (using a pristine slab, ethanol, water and H_2 as a reference and a potential of 0V/RHE) in function of the adsorption energy of atomic C and O respectively. The corresponding correlations are: $\Delta E(CH_3CO) = 0.40 \Delta E_C + 3.31$ and $\Delta E(CH_3COO) = 0.47 \Delta E_O + 2.95$. A typical geometry of acetyl and acetate are shown as an insert in their respective scaling graph.

Figure 4 compares the thermochemistry of the **Ox** and **Split** reactions for the series of transition metal surfaces under consideration. The reaction energies are computed at the equilibrium potential of the complete oxidation of ethanol into CO_2, namely 0.26V/RHE, which is most favorable for the competition since the **Ox** reaction is an electrochemical step and thus accelerated by overpotentials, while the desired **Split** reaction is not. Red lines divide three major zones: i) below the horizontal line ($\Delta E_{Ox} < 0$ eV), acetate formation is thermodynamically feasible while it is unfavorable above ($\Delta E_{Ox} > 0$ eV), ii) on the left side of the vertical line ($\Delta E_{split} < 0$ eV), the C–C bond cleavage is exothermic while it is endothermic on the right of this line, iii) the diagonal line reveals the thermodynamic selectivity of metals for oxidizing acetyl towards acetate with respect to C–C bond cleavage: metals above it favor C–C cleavage ($\Delta E_{Ox} > \Delta E_{Split}$) and vice versa. The ideal catalyst(s) would have been in the top left corner of Figure 4, which is unsurprisingly empty. This map shows that most metals are predicted to allow acetate formation. On several metals the C–C splitting is exothermic, but only a few are selective towards the C–C scission (Pd, Pt). These results are in line with the experimental results, where Pt and Pd have consistently been found to be most active for C–C splitting, although the CO_2 efficiency remains low.[4]
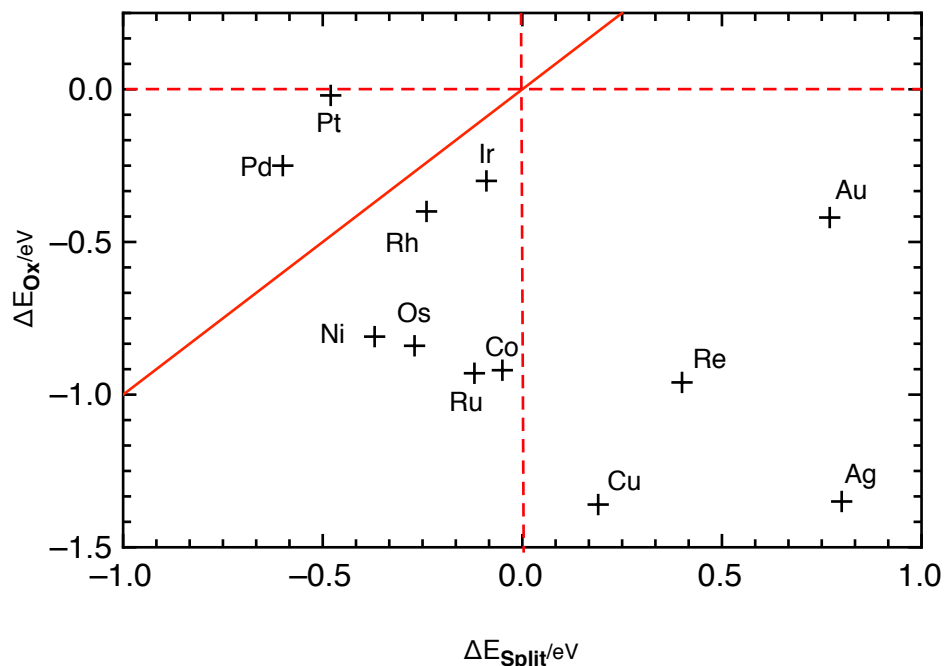
Figure 4. Reaction energy for the acetyl oxidation into acetate (ΔE_{Ox}) as a function of that of the C–C splitting in acetyl (ΔE_{Split}) at 0.26 V/RHE. Red dotted lines separate endothermic from exothermic zones and the red full line delimits the thermodynamic selectivity towards C–C splitting (top left corner).

The ability of a catalyst at cleaving acetyl into CO and methyl not only lies in the exothermicity of this dissociation but also in its activation energy E^a. Figure 5 shows this activation energy, E^a_{Split}, as a function of its corresponding reaction energy, ΔE_{Split}. In this plot, the best catalysts are located at the bottom left corner, i.e., metals on which the cleavage of the C–C bond is both exothermic and has the lowest activation energy. Based on this criterion, Co, Ni, Ru and Pd stand out as the best metals, featuring an activation energy lower than 1.1 eV. However, as shown in Figure 4, the oxidation of acetyl into acetate is strongly exothermic on Co, Ni, and Ru, leaving Pd as the most promising metal in agreement to available experimental data.[1,4]
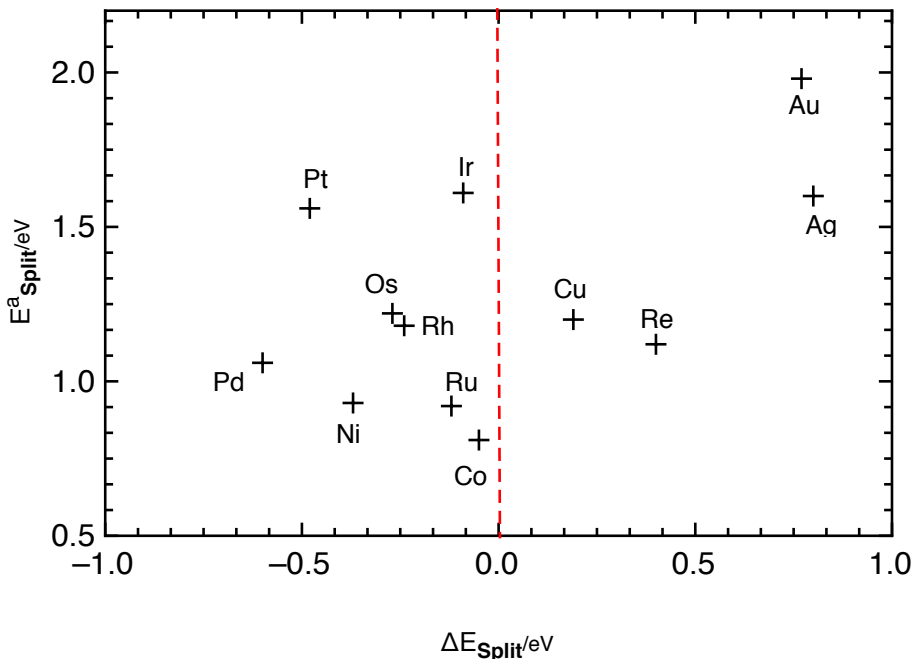
Figure 5. Activation energy (E^a_{Split}) in function of the reaction energy (ΔE_{Split}) of the C–C scission in adsorbed acetyl at 0.26 V/RHE for commonly used transition metals.

As already stated, the rapid oxidation of acetyl into acetate largely inhibits the full electro-oxidation of ethanol.[14] To extend the search beyond monometallic catalysts, the difference in stability between the unwanted acetate and the key acetyl intermediate $\Omega = \Delta E_{CH3CO} - \Delta E_{CH3COO}$ has to be expressed in function of simple descriptors. Since the binding energy of acetyl scales with the one of carbon E_c and the binding energy of acetate scales with the one of atomic oxygen E_O (see Figure 3 and its caption), this difference writes $\Omega(E_C, E_O) = [0.40 E_C - 0.47 E_O + 0.36 + 2*U]$ eV with a MAE of 0.11 eV. It is represented at 0.26V/RHE on Figure 6. The ideal catalyst should favor the splitting of the C–C bond rather than the oxidation of acetyl into acetate. In other words, Ω should be negative.
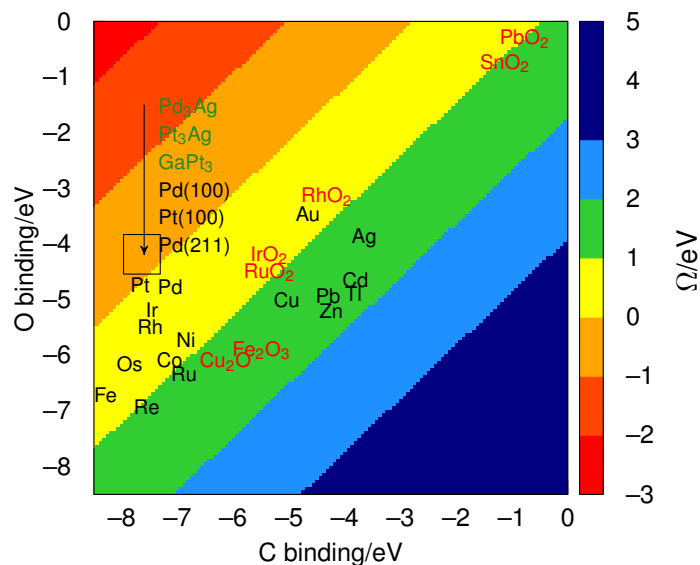
13

Figure 6: Expression of Ω as a function of the binding energy of C (ΔE_C) and O (ΔE_O) at 0.26V/RHE. The positions of the metals and of the oxides are indicated in black and red, respectively. The most promising alloys (e.g., AgPd$_3$ and AgPt$_3$, shown in green) are in same range as Pt/Pd(100), indicated by a square.

Exploiting Ω(E_C, E_O) in combination with the CatApp database,[31] more than 600 surfaces, for which E_C, E_O are available, have been screened. The set contains monometallics (Pb, Tl, Zn, etc), bimetallics (RuPt$_3$, PtRu$_3$, SnPt$_3$, etc) and intermetallics (Ni$_3$Al, etc).[30] The most promising surfaces were selected based on their predicted selectivity but also stability against oxidation, cost and toxicity and the lowest energy adsorption sites of C and O on those alloys were re-evaluated at our level of theory. As far as the monometallic catalysts are concerned, the most promising strategy seems to shape the nanoparticles into cubes since both Pd(100) and Pt(100) lie in the targeted region. Only a few of the bimetallics outperform Pd and Pt, with the most relevant ones being AgPd$_3$, AgPt$_3$ and GaPt$_3$ (see Table S4) all of which are clustered together in the same region as Pd(100) and Pd(100) on Figure 6. Since carbon is only weakly bound on Ag, neither the acetyl intermediate nor splitting the C–C bond is favorable over this metal (see Table S1/S3 and Figure 5) Therefore, monometallic Ag strongly favors acetate formation and it is interesting to note that, nevertheless, the Ag bimetallics afford rather promising catalysts.

With regards to metal oxides, which are likely to be formed under the oxidative conditions at the anode or would be added as catalyst supports, even the most expensive RhO_2 and IrO_2 are barely better than the much cheaper PbO_2 or SnO_2 as shown on Figure 6. Note that, like the screened metal surfaces we have considered pure metal oxides for C–C splitting, i.e., surfaces on which no hydroxyls are available. Hydroxyls are known to favor electrochemical steps (oxidation) rather than the chemical step (dissociation) and, on the other hand, block sites for adsorbing the intermediates, which are bound through the C atoms such as acetyl, CO and CH_x.

Conclusions

The challenge to develop efficient electrocatalysts for the full ethanol oxidation towards carbon dioxide has been analyzed in detail and explored by an *in-silico* screening. Acetic acid is found as the main obstacle: first, it is easily formed over most metals. Second, it can hardly be oxidized any further. To avoid acetic acid (acetate in alkaline media) formation, the C–C bond needs to be cleaved at the acetyl (CH_3CO) intermediate level. We show that activating the C–C bond in the key intermediate (acetyl) is challenging by itself ($E^a > 1$ eV for most metals) and is outcompeted by the electrochemical oxidation towards acetic acid. In terms of monometallic catalysts, the only promising metals are Pt and Pd, for which nanocubes preferentially exposing 100 facets would be most active and selective. Bimetallic and metal oxides catalysts are, according to our extensive screening, only of limited interest. Only a combination of Pt or Pd with Ag or Ga is competitive with Pt or Pd. Therefore, our study suggests that an orthogonal approach would be necessary in order to unleash the power of direct ethanol fuel cell. In particular, either the formulation of a catalyst able to oxidize acetate or the careful engineering of

the electrolyte and the exploitation of support effects could afford the much-needed leap towards full oxidation of ethanol.

Supplementary Materials: Tables with i) adsorption energies of C, O, CO, CH_3, CH_3CO and CH_3COO, ii) bond distances for CH_3CO on metal surfaces, and iii) reaction energies for acetyl, acetate, and C–C bond cleavage iv) data of Figure 5.

References
1. M. A. F. Akhairi and S. K. Kamarudin, *Int. J. Hydrogen Energy*, **41**, 4214–4228 (2016).
2. H. Chen, Y. Huang, D. Tang, T. Zhang, and Y. Wang, *Electrochim. Acta*, **158**, 18–23 (2015).
3. L. An, T. S. Zhao, and Y. S. Li, *Renew. Sustain. Energy Rev.*, **50**, 1462–1468 (2015).
4. Y. Wang, S. Zou, and W.-B. Cai, *Catalysts*, **5**, 1507–1534 (2015).
5. S. C. S. Lai et al., *Catal. Today*, **154**, 92–104 (2010).
6. C. Cremers et al., *ECS Trans.*, **16**, 1263–1273 (2008).
7. V. Rao, C. Cremers, and U. Stimming, *Fuel Cells*, **7**, 417–423 (2007).
8. X. Fang, L. Wang, P. K. Shen, G. Cui, and C. Bianchini, *J. Power Sources*, **195**, 1375–1378 (2010).
9. D. A. Cantane and F. H. B. Lima, *Electrocatalysis*, **3**, 324–333 (2012).
10. P. A. Christensen, S. W. M. Jones, and A. Hamnett, *J. Phys. Chem. C*, **116**, 24681–24689 (2012).
11. P. A. Christensen, A. Hamnett, and D. Linares-Moya, *Phys. Chem. Chem. Phys.*, **13**, 11739–11747 (2011).
12. P. A. Christensen and D. Linares-Moya, *J. Phys. Chem. C*, **114**, 1094–1101 (2010).
13. J. K. Nørskov et al., *J. Phys. Chem. B*, **108**, 17886–17892 (2004).
14. E. A. Monyoncho et al., *ACS Catal.*, **6**, 4894–4906 (2016).
15. A. N. Geraldes et al., *J. Power Sources*, **275**, 189–199 (2015).
16. Y.-Y. Yang et al., *ACS Catal.*, **4**, 798–803 (2014).
17. Z.-Y. Zhou, Q. Wang, J.-L. Lin, N. Tian, and S.-G. Sun, *Electrochim. Acta*, **55**, 7995–7999 (2010).
18. V. Rao et al., *J. Electrochem. Soc.*, **154**, 1138 (2007).

19. Z.-Y. Zhou and S.-G. Sun, *Electrochim. Acta*, **50**, 5163–5171 (2005).
20. P. Ferrin et al., *J. Am. Chem. Soc.*, **131**, 5809–5815 (2009).
21. J. E. Sutton and D. G. Vlachos, *Ind. Eng. Chem. Res.*, Ahead of Print (2014).
22. E. A. Monyoncho et al., *ChemElectroChem*, **3**, 218–227 (2016).
23. H. T. Zheng, Y. Li, S. Chen, and P. K. Shen, *J. Power Sources*, **163**, 371–375 (2006).
24. S. Tauster, *J. Catal.*, **55**, 29–35 (1978).
25. S. J. Tauster, S. C. Fung, and R. L. Garten, *J. Am. Chem. Soc.*, **100**, 170–175 (1978).
26. G. Kresse and J. Furthmüller, *Phys. Rev. B*, **54**, 11169–11186 (1996).
27. J. P. Perdew, K. Burke, and M. Ernzerhof, *Phys. Rev. Lett.*, **77**, 3865–3868 (1996).
28. G. Kresse and D. Joubert, *Phys. Rev. B*, **59**, 1758–1775 (1999).
29. M. Methfessel and A. T. Paxton, *Phys. Rev. B*, **40**, 3616–3621 (1989).
30. F. Studt et al., *J. Catal.*, **293**, 51–60 (2012).
31. J. S. Hummelshøj, F. Abild-Pedersen, F. Studt, T. Bligaard, and J. K. Nørskov, *Angew. Chemie Int. Ed.*, **51**, 272–274 (2012).
32. B. Gralec, A. Lewera, and P. J. Kulesza, *J. Power Sources*, **315**, 56–62 (2016).
33. A. Calderón-Cárdenas et al., *J. Braz. Chem. Soc.* (2014).